2007 IEEE International Conference on
Robotics and Automation
Roma, Italy, 10-14 April 2007

Benchmark of the 3-DOF Gantry-Tau Parallel Kinematic Machine

Geir Hovland
Agder University College
N-4898 Grimstad, Norway
Email: geir_hovland@ieee.org

Martin Choux & Matthew Murray
School of Inf.Tech & Elec.Eng
The University of Queensland
Brisbane, Australia QLD 4072

Torgny Brogårdh
ABB Robotics
SE-721 68 Västerås, Sweden
Email: torgny.brogardh@se.abb.com

***Abstract*— In this paper the invited session and the 4 original contributions are described first. Then the details of the first paper in the invited session is presented. In this first paper a new method for calculating the dynamic stiffness (frequency response) of parallel kinematic machines (PKMs) with six links, or Hexapods, is presented. The method assumes that each link and universal joint can be described by a mass-spring-damper model and calculates the transfer function from a Cartesian force or torque to Cartesian position or orientation. The new method has been used to benchmark two versions of the Gantry-Tau PKM, a relatively new PKM which has been designed to achieve a large workspace to installation space ratio, while at the same time achieve higher static and dynamic stiffness compared to serial-type industrial robots. The benchmark results presented in this paper show that these goals can be achieved in large sections of the workspace envelope. The benchmark also shows that machining centre specifications can be met if the location and dimensions of the work objects are known at the design stage.**

I. Invited Session

Session title: A Common Benchmark of a Group of Parallel Kinematic Machines

Original contributors: T. Brogårdh, C. Budde, D. Chablat, M. Choux, V. Duchaine, S. Foucault, C. Gosselin, J. Hesselbach, G. Hovland, X. Kong, P. Last, M.T. Masouleh, M. Murray, A. Pashkevich, P.-L. Richard, P. Wenger

The study of parallel kinematic machines (PKMs) has been an active research field in robotics and mechanical design for more than two decades. However, these machines have not yet got any broader use in industrial applications. One of the few designs that have made an impact in industry is the Delta robot by Clavel, [1]. The Delta robot has been successful in fast pick-and-place applications. However, the use of the Delta robot is restricted to applications where a small workspace to footprint ratio can be accepted.

The idea of using PKMs as CNC-type machine tools emerged during the early and mid 1990's. Fassi and Wiens [2] presented an overview of both industrial and university prototypes of PKM machine tools. Most of the existing PKM machine tools were developed in Europe, with the remainder developed in North America and Asia. It was early realised that PKM machine tools have many advantages, such as high payload to load ratio, noncumulative joint errors, high structural rigidity, modularity, location of motors at the fixed base and simple solutions of the inverse kinematics problem. However, as research continued the drawbacks of PKM machine tools also emerged: singularities inside the workspace, nonuniform Cartesian stiffness and resonance frequencies, complicated forward kinematics, complicated calibration strategies, often a limited workspace and difficulties to obtain joint stiffness and accuracy. The scientific community is currently strongly divided between supporters and those who think that PKM machine tools do not have a future. One critical article of PKMs was presented by [3]. They show that a chosen hexapod structure does not yet meet the specifications of a high-speed 5-axis machining centre.

It is still too early to conclude if high-speed machine tool applications will be too difficult for PKMs. On the other hand, there are still a large number of other application areas which would benefit from the advantages PKM structures have over their serial robot counterparts. It can be argued that high-performance machine tool applications have received too much attention from the PKM scientific community. Currently, there exist large gaps between the stiffness and dynamic properties of serial-type robots and many of the developed PKM prototypes. An industrial serial-type robot typically has a Cartesian stiffness in the range 1-2 Newtons per micron ($N/\mu m$) and resonance frequencies below 10 Hz. A high-speed machining centre typically has stiffness larger than $50N/\mu m$ and resonance frequencies larger than 50 Hz. Between these specifications there exists a large range of untapped application areas for PKMs. With higher stiffness and resonance frequencies compared to serial robots, PKMs can provide benefits such as reduced oscillations and overshoots which in turn can lead to economic benefits gained from reduced cycle-times.

During the last ten years a new group of PKMs has emerged. These machines use linear actuators at the robot base to increase and overcome one of the main limitations of PKMs in the past - the small workspace to footprint ratio. In this invited session several of these new PKMs are presented and for the first time benchmarked against a common set of criteria, including workspace, degrees of freedom, stiffness, singularities and dynamic properties. The goal of this invited session is to establish a current baseline of PKM performance which other researchers can challenge and improve in the future. In order to ease the comparison of the different machine concepts and to establish a benchmark for future comparison, a standard set of joints and links have been chosen by all the participants in the invited session.

The invited session contains the following PKM structures: The Tripteron, Quadrupteron and Pentapteron from the Université Laval Canada, the Triglide from the Technische Universität Braunschweig Germany, the Orthoglide from IRCCyN France and the Gantry-Tau invented by ABB Robotics Sweden and prototyped at the University of Queensland.

The Tripteron and Quadrupteron robots are kinemati-

1-4244-0602-1/07/$20.00 ©2007 IEEE.

cally decoupled (or partially decoupled) parallel mechanisms based on fixed linear actuators. These robots arise from the systematic type synthesis of parallel mechanisms for translational and scara motions. They have been invented and developed at Université Laval. Because of their decoupling features, the Tripteron and Quadrupteron have no singularities inside their workspace and a very simple kinematic model. They are also insensitive to errors in most of their link lengths. In this invited session, the prototypes of the Tripteron and Quadrupteron built at Université Laval will be benchmarked against workspace to footprint ratio, Cartesian stiffness, lowest resonance frequency, singularities and sensitivity to geometric errors.

The Triglide robot has been developed as a test bed for the Collaborative Research Centre SFB 562 at the Technical University of Braunschweig. According to the main topic of this interdisciplinary research group the robot has been designed for high speed handling and assembly tasks. Its hybrid structure with four degrees of freedom offers the well-known Scara-type motions. The parallel part of the structure is based on the linear Delta [4] with three identical kinematic chains whose build-up and arrangement have been altered and optimized for the realization of a workspace enlargement approach. Based on the use of several workspaces going along with different assembly modes of the structure this procedure allows for a significant enhancement of the workspace to installation space ratio. In this invited session the kinematic structure of the Triglide is benchmarked against workspace to installation space ratio, translational stiffness and sensitivity to geometric errors.

The Orthoglide is a Delta-type PKM dedicated to 3-axis rapid machining applications that was originally developed at IRCCyN France in 2000-2001 to meet the advantages of both serial 3-axis machines (regular workspace and homogeneous performances) and parallel kinematic architectures (good dynamic performances and stiffness). This machine has three fixed parallel linear joints that are mounted orthogonally. The geometric parameters of the Orthoglide were defined as function of the size of a prescribed cubic Cartesian workspace that is free of singularities and internal collision. The interesting features of the Orthoglide are a regular Cartesian workspace shape, uniform performances in all directions and good compactness. The entire Cartesian workspace is really available for tool paths. In this invited session, the Orthoglide is benchmarked according to geometric, kinematic and stiffness criteria : workspace to footprint ratio, condition number of the Jacobian matrix, sensitivity to geometric errors, torsional stiffness and translational stiffness.

The Tau family of robots was invented at ABB Robotics, Sweden in 2001. Tau robots are hexapods characterised by a grouping of the links in clusters of 1, 2 and 3. The Tau family also covers parallel and triangular mounted links. The Gantry-Tau prototyped at the University of Queensland is a special variant of this family, which uses linear actuators at the base and a triangular mounted link-pair. The triangular mounted pair allows for an extension of the reachable workspace of the robot while avoiding internal link and platform collisions. The Gantry-Tau is benchmarked against workspace to footprint ratio, translational stiffness, lowest resonance frequency, condition number of the link Jacobian and the sensitivity to geometric errors.

II. Introduction

The purpose of this paper is twofold. First, a new and general approach for calculating the dynamic frequency response of parallel kinematic machines (PKMs) with six links (Hexapods) is presented. This new method exploits the fact that this type of PKMs only experiences axial link forces and the method is significantly faster than general Finite Element (FE) methods used for other PKM structures which also take link bending and twisting moments into account. Second, a benchmark including five criteria is presented for two versions of the six-link Gantry-Tau PKM. The structure and kinematics of the Gantry-Tau have been presented before, for example in [5], [6], [7], but this paper presents for the first time a benchmark of the machine. The new general method for obtaining the frequency response of Hexapods PKMs is used in one of the benchmark criteria.

A frequency response model of a PKM over the entire working envelope is an essential tool when designing and dimensioning PKMs for high-speed machining and other applications. The flexibility of PKMs may cause structural resonance in the cutting process and mechanical interaction with the control system because of regenerative and modal chattering, which is the main concern in high-speed machining.

The majority of published works about PKM structures has been on kinematics and singularity analysis. The study of dynamics of PKMs has received less attention, and flexible dynamics less than rigid-body dynamics. One of the first published works on flexible PKM dynamics was presented by [8]. A 3-DOF spatial PKM with three flexible links was modelled and simulated. The model took both axial forces and bending moments into account. The model was only simulated in the time-domain, and no frequency response data was presented.

Two recent publications dealing with modelling of flexible PKMs were presented by [10], [11]. Both papers modelled Tripod PKMs with flexible links. Because of the Tripod structure, the flexible dynamic models must take link bending and twisting moments as well as axial forces into account. [11] presents a frequency response diagram of a Tripod and is able to quantify the lowest resonance frequency of the machine over the entire working envelope.

Very little work has been presented on flexible dynamic modelling of Hexapod PKMs. [9] is an example of a publication of a rigid-body dynamics model of a Hexapod. To our knowledge no general flexible links dynamics models which exploit the Hexapod structure have previously been published.

III. Static Stiffness Analysis

This section contains definitions and static relations which are required for the dynamic stiffness analysis in section IV.

The following notation is introduced: X, Y, Z are the Cartesian TCP coordinates, α, β, γ are the Cartesian TCP orientations, l_i and F_i where $i = 1, \cdots, 6$ are the six PKM link lengths and link forces, respectively. F_x, F_y and F_z are the external Cartesian forces acting on the TCP and M_x, M_y and M_z are the external Cartesian torques acting on the TCP, where TCP is defined in this paper as the tip of a milling tool located in the centre of the manipulated platform. The following vectors are then introduced

$$\begin{aligned} \mathbf{X} &= [X\ Y\ Z]^T & \theta &= [\alpha\ \beta\ \gamma]^T \\ \mathbf{F} &= [F_x\ F_y\ F_z]^T & \mathbf{M} &= [M_x\ M_y\ M_z]^T \\ \mathbf{L} &= [l_1\ l_2\ l_3\ l_4\ l_5\ l_6]^T & \mathbf{F}_a &= [F_1\ F_2\ F_3\ F_4\ F_5\ F_6]^T \end{aligned}$$

The relationship between the TCP forces and the link forces can then be expressed by the following two equations.

$$\mathbf{F} = \sum_{i=1}^{6} F_i \mathbf{u}_i \qquad \mathbf{M} = \sum_{i=1}^{6} F_i \mathbf{A}_i \times \mathbf{u}_i \tag{1}$$

where $\boldsymbol{u}_i$ is a unit vector in the direction of link i and $\boldsymbol{A}_i$ is a vector pointing from the TCP to the platform-side end-point of link i. The two equations above can be rewritten using the 6×6 statics matrix $\boldsymbol{H}$ as follows (left).

$$\begin{bmatrix} \mathbf{F} \\ \mathbf{M} \end{bmatrix} = \mathbf{H}\mathbf{F}_a \qquad \begin{bmatrix} \mathbf{\Delta X} \\ \mathbf{\Delta}\theta \end{bmatrix} = \mathbf{J}\mathbf{\Delta L} \tag{2}$$

The Jacobian matrix of the PKM relates changes in Cartesian position and orientation with changes in the link lengths as shown in eq.(2) (right) where the vectors $\mathbf{\Delta X}$ and $\mathbf{\Delta}\theta$ represent small changes in Cartesian position and orientation, the vector $\mathbf{\Delta L}$ represents small changes in the link lengths. This particular Jacobian should not be confused with the robot Jacobian which relates Cartesian velocities with the actuator velocities. Gosselin [12] showed the duality between the statics and the link Jacobian for PKMs, ie.

$$\mathbf{H}^{-1} = \mathbf{J}^T \tag{3}$$

Based on the duality result, the Cartesian stiffness matrix $\boldsymbol{K}$ can be derived as a function of the statics matrix as follows.

$$\begin{aligned} \begin{bmatrix} \mathbf{F} \\ \mathbf{M} \end{bmatrix} &= \boldsymbol{K} \begin{bmatrix} \mathbf{\Delta X} \\ \mathbf{\Delta}\theta \end{bmatrix} = \mathbf{H}\mathbf{F}_a = \mathbf{H}\boldsymbol{K}_L\mathbf{\Delta L} \\ &= \mathbf{H}\boldsymbol{K}_L\mathbf{J}^{-1} \begin{bmatrix} \mathbf{\Delta X} \\ \mathbf{\Delta}\theta \end{bmatrix} = \mathbf{H}\boldsymbol{K}_L\mathbf{H}^T \begin{bmatrix} \mathbf{\Delta X} \\ \mathbf{\Delta}\theta \end{bmatrix} \\ \Rightarrow \quad & \mathbf{K} = \mathbf{H}\boldsymbol{K}_L\mathbf{H}^T \end{aligned} \tag{4}$$

where $\boldsymbol{K}_L$ is a 6×6 diagonal matrix with the individual link stiffnesses along the diagonal. The result in eq.(4) has the benefit that no matrix inversions are required to calculate the Cartesian stiffness, which means that the Cartesian stiffness can be calculated at all coordinates, including coordinates where $\mathbf{H}$ is singular.

IV. Dynamic Stiffness Analysis

In this section a new method for calculating the frequency response of any Hexapod PKM structure is presented. Fig. 1 shows typical PKM links with a universal joint at either end. The flexible model of a single link in Fig. 2 assumes that

Fig. 1. *Picture of typical PKM links with universal joints.*

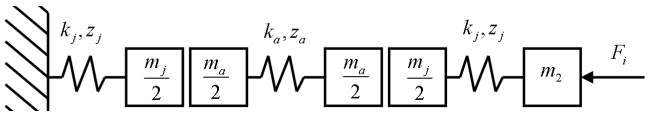

Fig. 2. *Flexible link model.*

the actuator is rigid and stationary as modelled by the fixed reference at the left-hand side of Fig. 2. For an accurate modelling of a link a number of serially connected masses and springs can be used. However, since usually a link is designed in such a way that the stiffness of the joint is much lower than the stiffness of the link a model as in Fig 2 will be a very good approximation.

The parameters k_j and damper z_j represent the flexibility in the universal joint. The mass m_j is the total weight of the joint. In Fig. 2 only half of the joint mass is used, as it is assumed that one half of the joint is rigidly attached to the stationary actuator. The mass m_a is the total weight of the link between the two universal joints. The two halves of the link weight are lumped together with the joint masses. The parameters k_a and z_a represent the link flexibility. The parameter m_2 represent the platform weight.

In the following the link arm of Fig. 2 is simplified to the model in Fig. 3. This simplification is made in this paper to reduce the complexity of the equations. Note, however, that the presented methods would also be applicable to the larger model of Fig. 2 without major modifications. In Fig. 3 the platform mass M_{TCP} equals the previous m_2 plus six halves of the joint masses, ie. $M_{TCP} = m_2 + 3m_j$. The mass M_a

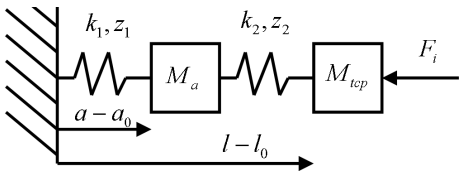

Fig. 3. *Simplified flexible link model.*

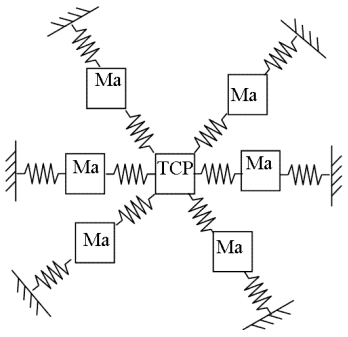

Fig. 4. *Flexible model of 6-link PKM.*

equals the sum of the masses of the two joint halves and the total weight of the link, ie. $M_a = m_a + m_j$. The new stiffness parameters in Fig. 3 are chosen the same ($k_1 = k_2$) and are calculated from the stiffness parameters of Fig. 2 such that the overall static stiffness is the same, ie.

$$\frac{1}{k_1} + \frac{1}{k_2} = \frac{2}{k_1} = \frac{2}{k_j} + \frac{1}{k_a} = \frac{2k_a + k_j}{k_a k_j} \quad (5)$$

$$k_1 = \frac{2k_a k_j}{2k_a + k_j} \quad (6)$$

Notice that $k_1 = k_j$ (the stiffness in the simplified model equals the joint stiffness) if $k_a >> k_j$, which is usually the case. Isolating the dynamics for link i and then the platform, the flexible equations of motion become

$$M_a \ddot{a}_i = -k_1 a_i - z_1 \dot{a}_i + (l_i - a_i)k_2 + (\dot{l}_i - \dot{a}_i)z_2 \quad (7)$$

$$M_{TCP}\ddot{\boldsymbol{X}} = \boldsymbol{F} + \sum_j (a_j - l_j)k_2 \boldsymbol{u}_j + \sum_j (\dot{a}_j - \dot{l}_j)z_2 \boldsymbol{u}_j \quad (8)$$

$$I_{TCP}\ddot{\boldsymbol{\theta}} = \boldsymbol{M} + \sum_j (a_j - l_j)k_2(\boldsymbol{A}_j \times \boldsymbol{u}_j) + \sum_j (\dot{a}_j - \dot{l}_j)z_2(\boldsymbol{A}_j \times \boldsymbol{u}_j) \quad (9)$$

where $\boldsymbol{u}_j$ and $\boldsymbol{A}_j$ were introduced in eq.(1). For small motions, the equations above are linear in the variables a, l as functions of the external TCP forces $\boldsymbol{F}$ and torques $\boldsymbol{M}$ and the TCP linear and rotary accelerations. By introducing the Laplace transform, the 18 equations above can be written on matrix form as follows.

$$\begin{bmatrix} A & -B \\ C & D \end{bmatrix} \begin{bmatrix} a_i \\ l_i \end{bmatrix} = \begin{bmatrix} \mathbf{0} \\ \boldsymbol{F} \\ \boldsymbol{M} \end{bmatrix} \quad (10)$$

where $\mathbf{0}$ is a 6×1 zero vector. The matrix elements A, B, C and D are functions of the Laplace transform, the masses and the flexibility parameters. For example,

$$A = \left(M_a s^2 + (z_1 + z_2)s + k_1 + k_2\right)\boldsymbol{I}_6 \quad (11)$$

$$B = (z_2 s + k_2)\boldsymbol{I}_6 \quad (12)$$

where $\boldsymbol{I}_6$ is a 6×6 identity matrix. In addition to the link masses, springs and dampers, the 6×6 sub-matrices C and D will also contain platform parameters, such as the platform weight and inertia. The Cartesian position vector $\boldsymbol{X}$ and the orientation vector $\boldsymbol{\theta}$ are replaced by a and l by using the Jacobian matrix. The expressions for C and D are too lengthy to show in this paper.

Hence, the 12 unknown parameters a_i and l_i can be solved by inverting the matrix in eq. (10). If we know the direct link Jacobian matrix of the PKM, the Cartesian velocities can be calculated as follows.

$$\begin{bmatrix} \dot{\boldsymbol{X}} \\ \dot{\boldsymbol{\theta}} \end{bmatrix} = \boldsymbol{J}\dot{\boldsymbol{L}} \rightarrow s\boldsymbol{I}_6 \begin{bmatrix} \boldsymbol{X} \\ \boldsymbol{\theta} \end{bmatrix} = s\boldsymbol{I}_6 \boldsymbol{J}\boldsymbol{L} \quad (13)$$

where $\boldsymbol{L} = [l_1, \cdots, l_6]^T$. The final transfer functions of the PKM from Cartesian forces or moments to Cartesian positions or orientation can then be derived from eqs.(10) and (13).

$$\frac{\boldsymbol{X}_i}{F_j}(s) = \frac{\boldsymbol{X}_i}{l_i}(s)\frac{l_i}{F_j}(s) \qquad \frac{\boldsymbol{\theta}_i}{M_j}(s) = \frac{\boldsymbol{\theta}_i}{l_i}(s)\frac{l_i}{M_j}(s) \quad (14)$$

Bode plots can be generated by replacing the Laplace transform s by $\jmath\omega$, where $\jmath$ is the complex unity and ω a frequency and solving the set of 12 equations above for a range of different frequencies. Note that if the more detailed model of Fig. 2 was chosen, a set of 18 equations would have to be solved for each frequency.

V. Computational Efficiency

In [5] an approach to calculate the Cartesian stiffness was presented using the forward kinematics. For many PKMs the forward kinematics can be difficult to calculate and must be calculated in numeric form. Numeric solutions are often computationally expensive. A second approach to calculating stiffness is to use the Jacobian matrix derived from the inverse kinematics and matrix inversion. A third approach is to avoid any matrix inversions and calculate the stiffness from eq. (4) by using the statics matrix. Table I shows the computational requirements for the three different approaches on the triangular version of the 3-DOF Gantry-Tau PKM described in [5], [7]. The computing time has been normalised to 1 for the third approach. The results in

Method	Time
Numerical forward kinematics	500
Jacobian matrix $\boldsymbol{J}$	6.66
Static matrix $\boldsymbol{H}$	1

TABLE I

Static stiffness computation time for three different methods.

Table I are based on a Cartesian stiffness calculation over a grid covering the entire workspace of the PKM and in all force directions. The method based on the static matrix $\boldsymbol{H}$ is 500 times faster than the method based on the numerical forward kinematics. Similar computational benefits by using the statics matrix are found when computing resonance frequencies and singularities, which makes the frequency response methods presented in this paper significantly faster than alternative FE methods.

VI. Benchmark: The 3-DOF Gantry-Tau

In this section two 3-DOF versions of the Gantry-Tau are benchmarked. The first version has 5 fixed links lengths of $1.0m$ and one single telescopic actuator as illustrated in Fig. 5. The second version of the machine has all 6 link lengths fixed at $1.0m$. The second version of the machine has been presented before in [5], [6], [7] and a more detailed kinematic description of the machine can be found in those papers.

Both versions of the machine have 3 main linear actuators, which are aligned in the positive Cartesian X direction. The actuators have 1, 2, and 3 links attached, respectively, and the name Tau arises from this configuration. The variable actuator positions in the X-direction are denoted q_1, q_2 and

q_3 and have lower and upper bounds at 0 and $2.2m$. The Y and Z coordinates of the actuators are fixed and are given by: $Y_1 = -Q$, $Z_1 = Q$, $Y_2 = 0$, $Z_2 = 2Q$, $Y_3 = 0$ and $Z_3 = 0$, where $Q = 0.5m$.

The telescopic version of the machine is presented and analysed for the first time in this paper. The telescopic link length is actively controlled such that $q_1 = X$, which makes the link as short as possible. As will be presented in this section, a short telescopic link improves several of the benchmark criteria, such as workspace, stiffness and resonance frequencies. Note that the fixed-length version is in a singular position when $q_1 = X$, while the telescopic version is not. For the telescopic version, motion in the positive Y-direction is still possible by extending the length of the telescopic leg.

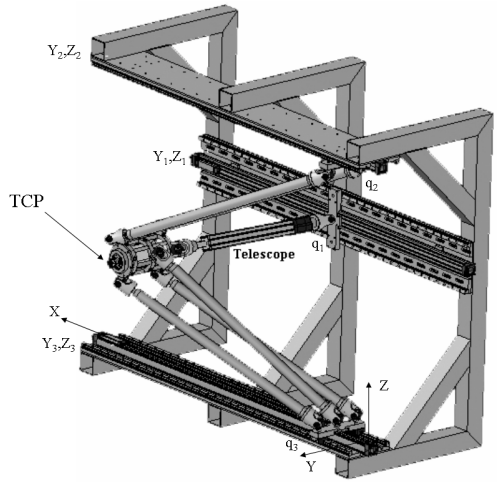

Fig. 5. *The Gantry-Tau robot with one telescopic actuator.*

A. Benchmark: Workspace to Installation Space Ratio

The dimensional parameters for the support frame of the two versions of the Gantry-Tau are as follows: $2.2m$ (width), $0.5m$ (depth) and $1.0m$ (height). Hence, the smallest room in which the robot would fit is $1.1m^3$. Because of the triangular link-pair design of the Gantry-Tau, the machine can be reconfigured as illustrated in Fig. 6, which increases the reachable workspace at either end of the linear actuators. When replacing the triangular link pair with a parallel link pair, it will be much more difficult to design the moving platform to avoid internal collisions with the links for both configurations. The total 3-DOF workspace of the Gantry-Tau with the dimensions above and all 6 link lengths fixed at 1.0 metres is $3.02m^3$. The total workspace of the Gantry-Tau version with one telescopic link as illustrated in Fig 6 is $3.44m^3$. For the telescopic version, the telescopic link length varies between $0.06m$ and $1.11m$. In practice it may be difficult to achieve the short length of $0.06m$ for the telescope link. If the telescope link has a lower limit larger than $0.06m$, then the workspace will be in the range between 3.02 and $3.44m^3$. Workspace points where the tool platform collides with the support frame have been removed and the Gantry-Tau has no internal link collisions with the dimensions

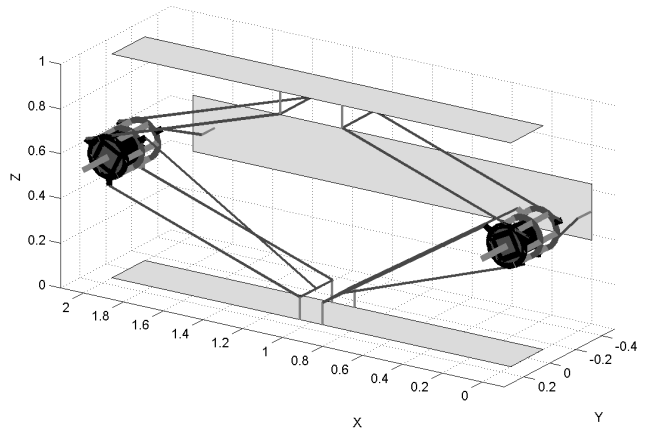

Fig. 6. *Illustration of the Gantry-Tau in both left and right-handed configuration.*

chosen. Hence, the total workspace to installation space ratios of the two versions of the machine are 2.75 and 3.13. The workspace to installation space ratio of the machine will always be larger than one, since the tool platform can extend beyond the actuator limits. As the length of the linear actuators increase, the workspace ratio will approach one.

B. Benchmark: Cartesian Stiffness

The minimum, maximum and average Cartesian stiffnesses of the Gantry-Tau in the entire workspace and in the best 70% of the workspace are listed in Table II. Each of the 12 universal joints has a weight $1.0kg$ and a stiffness 50 N/μm. The stiffnesses of the support frame and the actuators are assumed infinite. The links have weight $1.0kg$ and stiffness $232N/\mu m$. The platform weight is $5kg$ and the inertia matrix I_{TCP} is a diagonal matrix with elements 0.06, 0.02 and 0.07. Fig. 7 shows the stiffness in the Cartesian Y-direction

Entire Workspace	X	Y	Z
Minimum	19.50	5.06	18.69
Maximum	67.51	57.88	55.46
Average	53.20	22.28	29.36
Best 70% Workspace	X	Y	Z
Minimum	49.37	13.81	22.55
Maximum	67.51	57.88	55.46
Average	59.13	27.70	33.08

TABLE II

Cartesian stiffnesses (N/μm) of the Gantry-Tau with one telescopic link in the entire workspace and the best 70% workspace.

as a function of the Y and Z coordinates at $X = 1.0$ for the telescopic link version of the machine. The stiffness is well-defined with no discontinuities in the entire workspace, which is also the case for the stiffnesses in the X and Z directions. Note in Fig. 7 that the stiffness in the Y-direction is well over $100N/\mu m$ for coordinates where $Y > 0.6$, which is often the most useful area of the workspace. The stiffness in the Y-direction is lowest where the Y coordinates are close to zero.

Note that the telescopic link version of the machine more than triples the Cartesian stiffness in the Y-direction

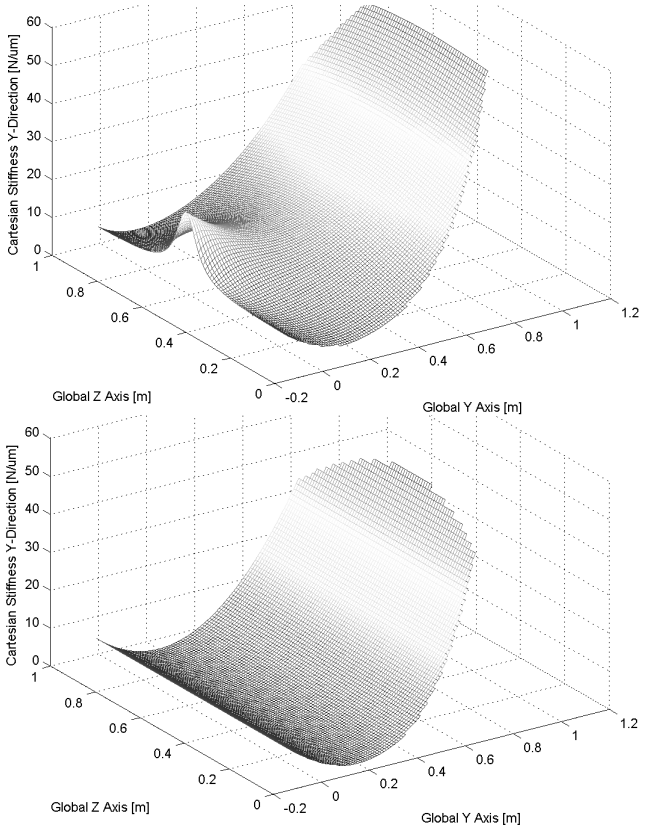

Fig. 7. *Cartesian stiffness in the Y-direction as function of the Y and Z coordinates at $X = 1.0$: Telescopic version (top) and fixed link length version (bottom).*

Entire Workspace	X	Y	Z
Minimum	26.59	2.05	19.02
Maximum	82.82	50.90	42.29
Average	65.49	13.04	26.32
Best 70% Workspace	X	Y	Z
Minimum	60.56	3.89	21.45
Maximum	82.82	50.90	42.29
Average	72.76	17.48	28.89

TABLE III

Cartesian stiffnesses (N/μm) of the Gantry-Tau with fixed link lengths in the entire workspace and the best 70% workspace.

compared to the fixed link length version in the best 70% workspace, without dramatically reducing the stiffness in the other directions. Because of the single link, the Y-direction is the weakest direction of the machine. Note however that at the extremes of the workspace in the X directions, q_1 can no longer be chosen equal to X because of the actuator limits for the telescopic link version of the machine. At these workspace boundaries, the stiffness values of the telescopic version will approach the values for the fixed link length machine.

C. Benchmark: Resonance Frequency

Fig. 8 shows two examples of the frequency response curves that are generated by the methods in Section IV. The solid curve shows the amplitude response from a Cartesian force in the X-direction to Cartesian position in the X-direction at $X = 1.0$, $Y = 0.0$ and $Z = 0.5$. The dotted curve shows the same response at $X = 1.0$, $Y = 0.8$ and $Z = 0.5$. The first resonance frequency occurs at 322 rad/sec or 51.2 Hz and 525 rad/sec or 83.6 Hz, respectively, for the two selected locations. The minimum, maximum and

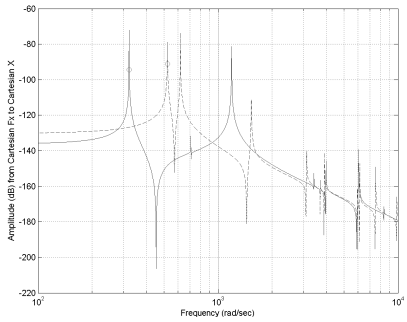

Fig. 8. *Example of frequency response curves for the fixed-length version of the Gantry-Tau.*

average first resonance frequency of the two versions of the Gantry-Tau in the entire workspace and the best 70% of the workspace are listed in Table IV. A map of the first resonance

	Min	Max	Avg
Telescopic: entire workspace	29.37	109.46	93.64
Telescopic: best 70% workspace	93.58	109.46	100.10
Fixed-length: entire workspace	47.54	102.85	60.61
Fixed-length: best 70% workspace	53.84	102.85	64.43

TABLE IV

Resonance frequencies of the two versions of the Gantry-Tau.

frequency as a function of the Y and Z coordinates for the telescopic version of the machine (top) and the fixed link length version (bottom) are shown in Fig. 9. The resonance maps of the two machines are similar, with the resonance frequencies of the telescopic version slightly larger than for the fixed link length version. The robot configurations in the positions with the lowest and highest resonance frequencies for the telescopic version of the machine are shown in the YZ-plane in Fig. 10. The lowest resonance frequency of 29.37 Hz occurs at the position $Y = -0.10$, $Z = 0.20$. At this location the condition number (smallest divided by largest singular value) of $\mathbf{J}$ is 0.0485. The large resonance frequency of 109.46 Hz occurs at the position $Y = 0.25$ and $Z = 0.90$. At this location the condition number of $\mathbf{J}$ is 0.0616. The frequency response data generated by the new method presented in this paper have been verified against calculations from a FE software package (Strand7). For a set of 10 locations in the workspace of the Gantry-Tau, the method in this paper generates the same results as the FE package and the method is also significantly faster. The maps in Fig. 9 can be generated approximately in the same time as it takes to set up and calculate one resonance frequency in a FE package.

D. Benchmark: Condition Number of Statics Matrix

The minimum, maximum and average condition number (smallest divided by largest singular value) of the statics ma-

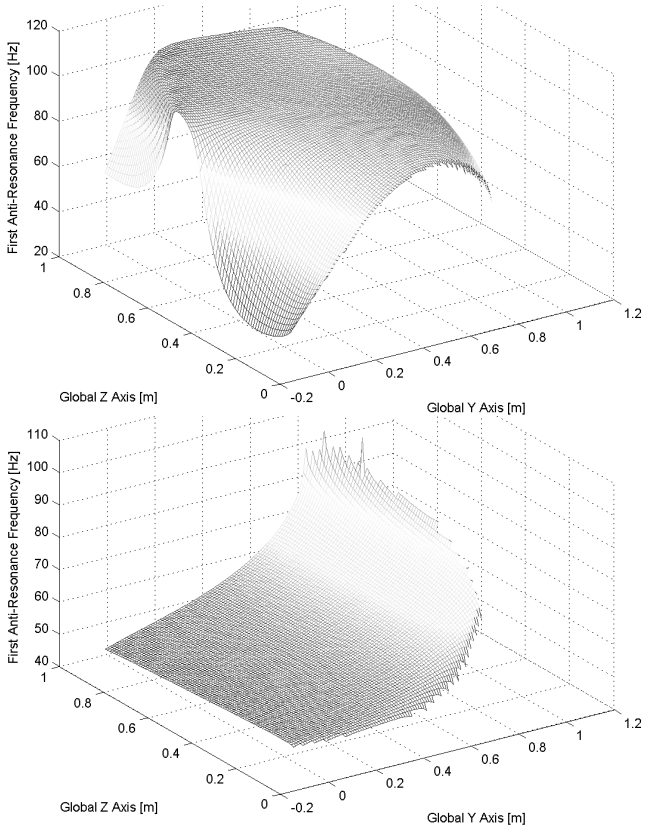

Fig. 9. *First resonance frequency as function of the Y and Z coordinates at $X = 1.0$: Telescopic version (top) and fixed link length version (bottom).*

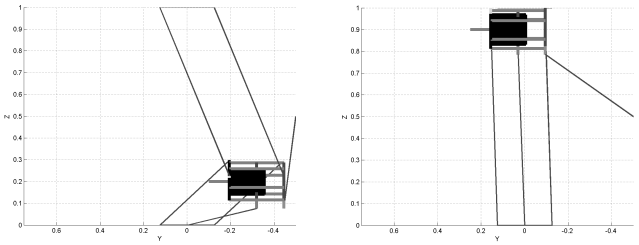

Fig. 10. *Robot configurations with the lowest (left, 29.37 Hz) and highest (right, 109.46 Hz) resonance frequencies shown in the YZ-plane.*

trix $\mathbf{H}$ in the best 70% of the workspace are listed in Table V. The results in Table V and Fig. 11 show similar results for the two versions of the Gantry-Tau. The telescopic version of the machine has the largest variations in this benchmark criterion. The statics matrix $\boldsymbol{H}$ has no singularities inside the workspace for a given assembly mode (configuration) of the robot. The Gantry-Tau will have singularities when arms 2 and 3 are parallel and in different assembly modes, but this case is not considered in this benchmark.

E. Benchmark: Sensitivity to Geometric Errors

The minimum, maximum and average worst-case Cartesian displacements in the entire and best 70% of the workspace as functions of a $\pm 1mm$ error in each of the fixed link lengths are listed in Table VI. The results show that the telescopic version is less sensitive to link length

Machine	Min	Max	Average
Telescopic Entire Workspace	0.0388	0.0933	0.0587
Telescopic Best 70%	0.0558	0.0933	0.0625
Fixed Links Entire Workspace	0.0422	0.0802	0.0550
Fixed Links Best 70%	0.0520	0.0802	0.0575

TABLE V

Condition numbers of the statics matrix.

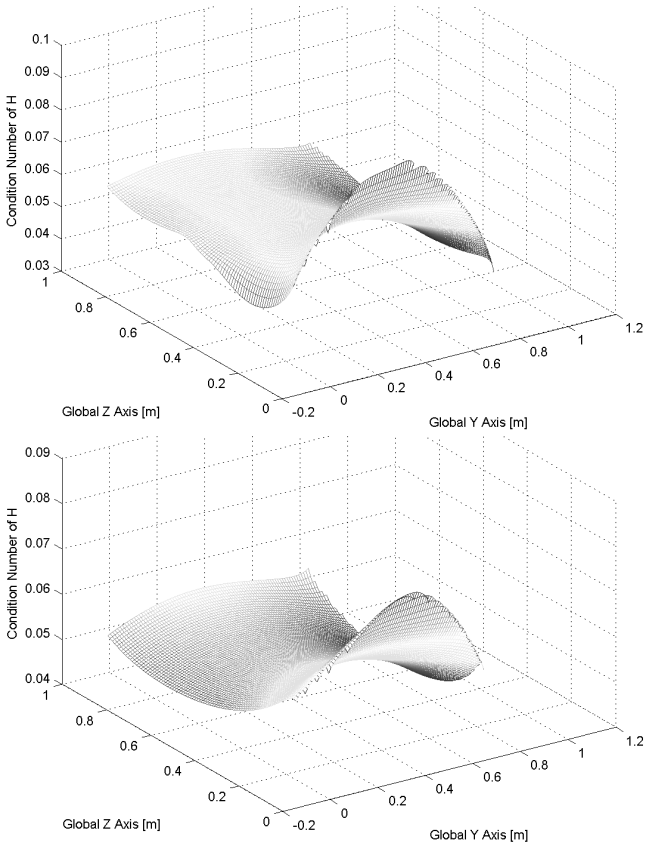

Fig. 11. *Condition number of the statics matrix $\mathbf{H}$ for telescopic version (top) and fixed length link version (bottom).*

errors in the best 70% of the workspace, particulary in the Y-direction. The maximum sensitivity of the telescopic version is a factor of 1.52 in the Z direction. The fixed link length version of the machine has a maximum sensitivity of 2.69 in the Y direction in the best 70% of the workspace. Note that the telescopic version of the machine has relatively large sensitivities (5.05) at the back of the workspace $(Y = -0.1)$ as seen in Fig. 12. This area is not usually used for machining operations, but can be used as a transfer area to avoid collisions with workpieces. The fixed link length version does not have these large sensitivities.

VII. Conclusions

In this paper a new general method for calculating the frequency response of Hexapod PKM structures is presented. The method considers flexible links and universal joints. The model allows PKM resonance maps such as in Fig. 9 to be generated in very short time compared to FE software packages.

Telescopic: Entire workspace	X	Y	Z
Minimum	0.65	0.99	1.12
Maximum	2.07	5.05	2.02
Average	1.09	1.31	1.47
Telescopic: best 70% workspace	X	Y	Z
Minimum	0.65	0.99	1.12
Maximum	1.14	1.29	1.51
Average	0.91	1.09	1.40
Fixed-length: Entire workspace	X	Y	Z
Minimum	0.66	1.29	1.16
Maximum	1.70	2.81	1.82
Average	1.17	2.43	1.46
Fixed-length: best 70% workspace	X	Y	Z
Minimum	0.66	1.29	1.15
Maximum	1.30	2.69	1.52
Average	1.08	2.30	1.39

TABLE VI

Worst-case Cartesian displacement sensitivity (mm) to a $\pm 1mm$ error in each of the link lengths.

A benchmark of two versions of the Gantry-Tau PKM structure has been presented for the first time. The results in this paper show that the benchmark criteria of the two versions of the Gantry-Tau are higher than for most serial-type industrial robots which have typical static stiffness values less than $2N/\mu m$ and the lowest resonance frequencies below 10 Hz. The benchmark results for the Gantry-Tau presented in this paper satisfy most of the specifications of typical machining centres, except for the stiffness in the Y direction. Typical machining centres have a uniform stiffness higher than $50N/\mu m$ and resonance frequencies higher than 50 Hz, see for example [3]. However, both versions of the Gantry-Tau satisfy the machining requirements in sections of the workspace, including the stiffness in the Y-direction, see Figs. 7 and 9.

A major benefit of the Gantry-Tau structure compared to a typical machining centre is the large workspace to installation space ratio that can be achieved. For the two versions of the Gantry-Tau benchmarked in this paper, the workspace to installation space ratio is close to a factor 3.

The benchmark results in this paper demonstrate the importance of designing PKMs in general and the Gantry-Tau in particular to meet specific end-user requirements. Both versions of the machine presented in this paper can satisfy high machining centre specifications, but only in parts of the workspace. It is therefore important that when the machine is designed, the locations of typical work-objects are known. The machine can then be designed for high performance in these regions. The remaining regions of the workspace with lower performance can typically be used for operations which do not require the machining specifications, such as tool change, docking or work object transfer operations.

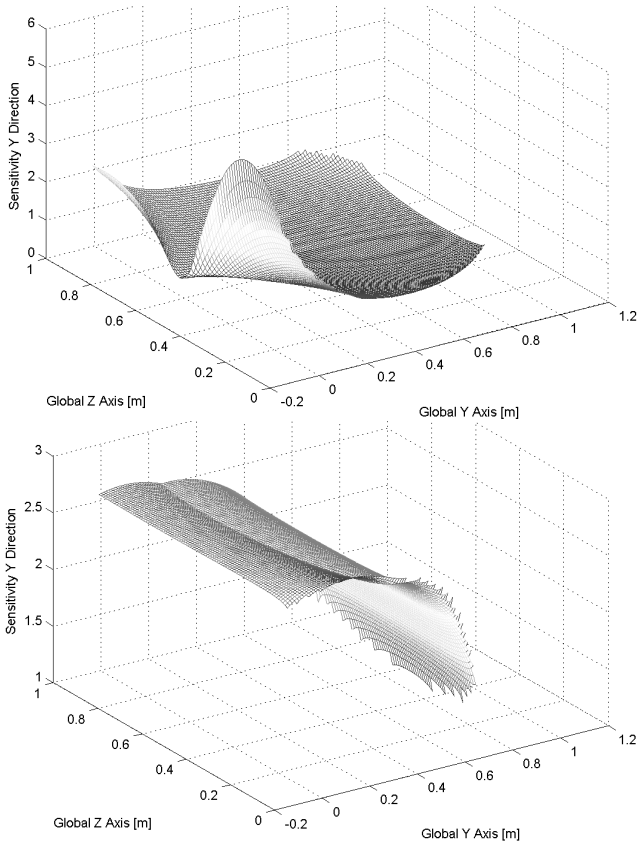

Fig. 12. *Cartesian sensitivity in the Y-direction: Telescopic version (top) and fixed link length version (bottom).*

REFERENCES

[1] R. Clavel, "DELTA, a fast robot with parallel geometry", Proc. of the International Symposium on Industrial Robots; Lausanne (Switzerland); 26-28 Apr. 1988. pp. 91-100.

[2] I. Fassi and G. Wiens, "Multiaxis Machining", Journal of Manufacturing Processes, Vol. 2, No. 1, 2000, pp. 1-14.

[3] J. Tlusty, J.C. Ziegert and S. Ridgeway, "A Comparison of Stiffness Characteristics of Serial and Parallel Machine Tools", *Journal of Manufacturing Processes*, Vol. 2, No. 1, pp. 67-76, 2000.

[4] R. Clavel, "Robots Parallèles, Techniques de l'Ingénieur, traité Mesures et Contrôle", Vol. R 7 710, 1994, pp. 1-8.

[5] T. Brogårdh, S. Hanssen and G. Hovland, "Application-Oriented Development of Parallel Kinematic Manipulators with Large Workspace", *Proc. of the 2nd International Colloquium of the Collaborative Research Center 562: Robotic Systems for Handling and Assembly*, Braunschweig, Germany, May 2005, pp. 153-170.

[6] M. Murray, G. Hovland and T. Brogårdh, "Collision-Free Workspace Design of the 5-Axis Gantry-Tau Parallel Kinematic Machine", *Proc. of the 2006 IEEE/RSJ Intl. Conference on Intelligent Robots and Systems*, Beijing, October 2006.

[7] I. Williams, G. Hovland and T. Brogårdh, "Kinematic Error Calibration of the Gantry-Tau Parallel Manipulator", *Proc. of the IEEE Intl. Conference on Robotics and Automation*, Orlando, May 2006.

[8] A. Fattah, J. Angeles and A.K. Misra, "Dynamics of a 3-DOF Spatial Parallel Manipulator with Flexible Links", *Proc. of the 1995 International Conference on Robotics and Automation*, pp.627-632.

[9] F. Xi, R. Sinatra and W. Han, "Effect of Leg Inertia on Dynamics of Sliding-Leg Hexapods", *Journal of Dynamic Systems, Measurement and Control*, Vol. 123, pp. 265-271, 2001.

[10] Z. Zhou, J. Xi and C.K. Mechefske, "Modeling of a Fully Flexible 3PRS Manipulator for Vibration Analysis", *Journal of Mechanical Design*, Vol. 128, pp. 403-412, 2006.

[11] J.S. Chen and W.Y. Hsu, "Dynamic and Compliant Characteristics of a Cartesian-Guided Tripod Machine", *Journal of Manufacturing Science and Engineering*, Vol. 128, pp. 494-502, 2006.

[12] C. Gosselin, "Stiffness Mapping for Parallel Manipulators", *IEEE Trans. on Robotics and Automation*, Vol. 6, No. 3, pp. 377-382, 1990.